Landslide susceptibility assessment of the region affected by the 25 April 2015 Gorkha earthquake of Nepal

Amar Deep Regmi[1]* http://orcid.org/0000-0002-1423-9990; e-mail: amardeep_regmi@yahoo.com

Megh Raj Dhital[2] http://orcid.org/0000-0002-8093-7658; e-mail: mrdhital@gmail.com

ZHANG Jian-qiang[1] http://orcid.org/0000-0003-3908-1082; e-mail: zhangjianqiang83@163.com

SU Li-jun[1] http://orcid.org/0000-0001-9972-4698; e-mail: sulijun1976@163.com

CHEN Xiao-qing[1] http://orcid.org/0000-0002-0177-0811; e-mail: xqchen@imde.ac.cn

* Corresponding author

1 Key Laboratory of Mountain Hazards and Earth Surface Process, Institute of Mountain Hazards and Environment, CAS, Chengdu 610041, China

2 Central Department of Geology, Tribhuvan University, Kirtipur 44613, Nepal

Abstract: Nepal was hit by a 7.8 magnitude earthquake on 25th April, 2015. The main shock and many large aftershocks generated a large number of coseismic landslips in central Nepal. We have developed a landslide susceptibility map of the affected region based on the coseismic landslides collected from remotely sensed data and fieldwork, using bivariate statistical model with different landslide causative factors. From the investigation, it is observed that most of the coseismic landslides are independent of previous landslides. Out of 3,716 mapped landslides, we used 80% of them to develop a susceptibility map and the remaining 20% were taken for validating the model. A total of 11 different landslide-influencing parameters were considered. These include slope gradient, slope aspect, plan curvature, elevation, relative relief, Peak Ground Acceleration (PGA), distance from epicenters of the mainshock and major aftershocks, lithology, distance of the landslide from the fault, fold, and drainage line. The success rate of 87.66% and the prediction rate of 86.87% indicate that the model is in good agreement between the developed susceptibility map and the existing landslides data. PGA, lithology, slope angle and elevation have played a major role in triggering the coseismic mass movements. This susceptibility map can be used for relocating the people in the affected regions as well as for future land development.

Keywords: Earthquake; Himalaya; Coseismic landslide; Susceptibility; bivariate statistical model; Nepal

Abbreviations: Himalayan Frontal Thrust (HFT), Main Boundary Thrust (MBT), Main Central Thrust (MCT), South Tibetan Detachment (STD), Great Midland Antiform (GMA), Peak Ground Acceleration (PGA)

Introduction

A devastating MW 7.8 Gorkha earthquake of April 2015 had its epicenter at Barpak, about 77 km NW of Kathmandu (Figure 1). The quake and its subsequent aftershocks were responsible for about
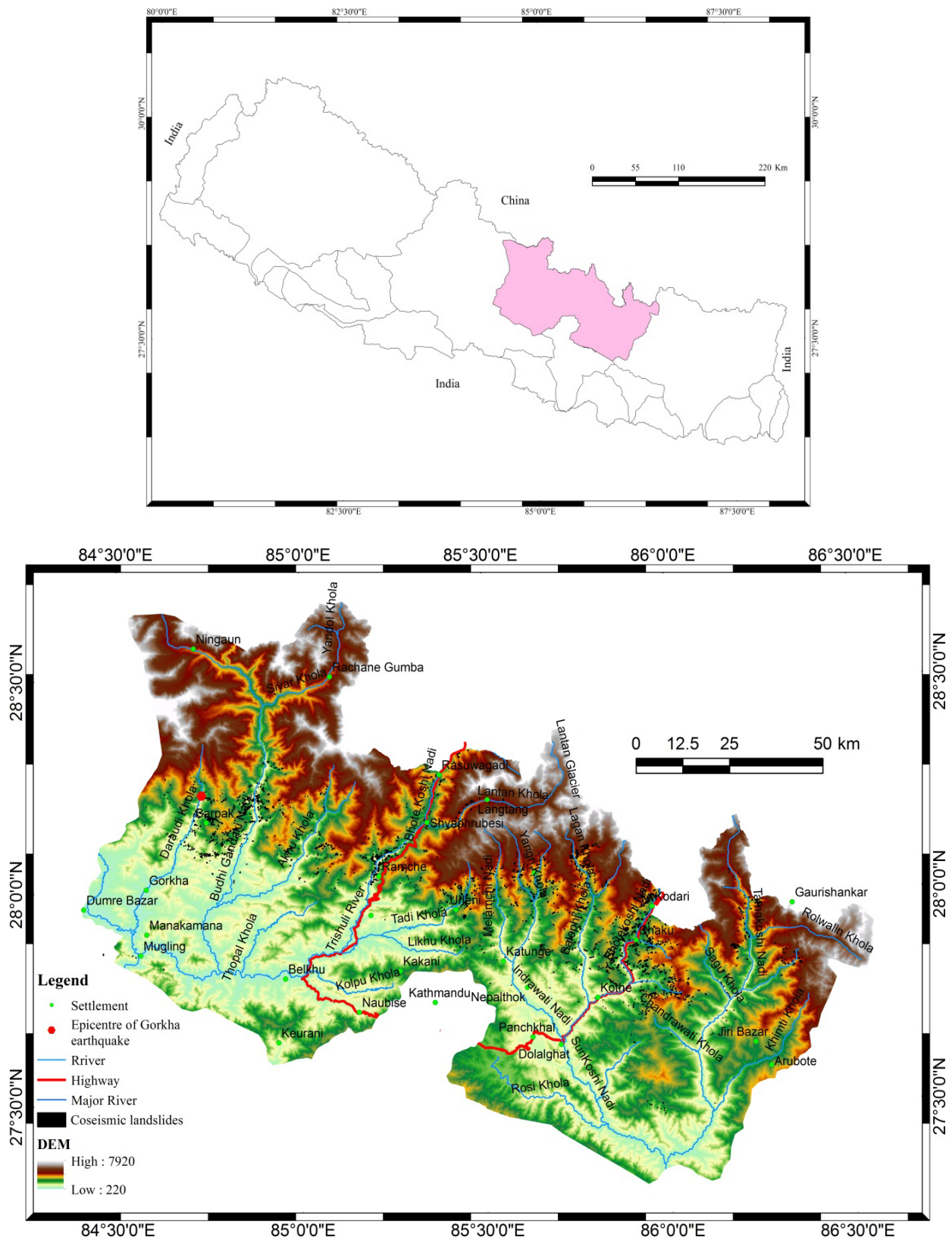
Figure 1 Map showing the location of the study area, (a) Map of Nepal showing the study area and the distribution of drainage basins in Nepal; (b) DEM of the study area, showing the distribution of coseismal landslide and major rivers.

9,000 deaths, 23,000 injuries, and a tremendous damage to the public and private property (MoHA 2015; Collins and Jibson 2015; Kargel et al. 2016). It became the worst natural disaster that struck Nepal after the 1934 Nepal–Bihar earthquake.

The earthquake is believed to reactivate the Main Himalayan Thrust, lying below the Main Central Thrust (MCT) in the central Nepal Himalaya, at a depth of about 15 km (USGS 2015). The low-angle (less than 10 degrees) rupture zone runs for a length of about 160 km from Barpak towards the east and it is about 80 km wide. It essentially follows the core of the Great Midland Antiform (GMA), running from west to east throughout the Nepal Himalaya and beyond (Hagen 1969; Dhital 2015).

Frequently, large earthquakes set off numerous landslips (Keefer 1984; Yin et al. 2009; Qi et al. 2010; Chigira et al. 2010) and the Gorkha earthquake was no exception. Its mainshock and many aftershocks brought about various mass movements in the mountainous areas of Nepal with rugged topography, high relief, steep slopes and deep valleys (Collins and Jibson 2015; Kargel et al. 2016; Regmi et al. 2016). The landslips killed more than 2,000 people in different parts of the country (MoHA, 2015). In the village of Ghodatabela and Langtang of Langtang Valley, a rock-snow avalanche swept about 329 people away, whereas more than 25 people lost their life at the Everest base camp by another snow avalanche related to the same quake. The most severely hit areas by the coseismic landslides are the settlements around Sindhupalchok, Gorkha, Rasuwa, Dhading, Nuwakot and Dolakha districts.

Landslide inventory is the most essential part in the susceptibility evaluation of an area (Guzzetti et al. 2012). Thus, for the susceptibility evaluation of earthquake induced landslides, it is important to prepare inventory map of coseismic landslides. Several researchers have done extensive research for developing landslide inventories of some earthquake affected regions. The first basic coseismic inventory map for Daly City was developed in 1957 after the California earthquake (Keefer 1984). Harp (1996) developed the first large inventory map for the 1976 Guatemala earthquake (Ms 7.5). Due to the development of several technologies as aerial photography, remote sensing techniques and GIS, the development of coseismic landslide inventory have become much easier. There are several literatures relating to the coseismic landslide inventories for major earthquakes as (Harp 1996; Lee et al. 2008; Khazai and Sitar 2004; Yamagishi and Iwahashi 2007; Chigira and Yagi 2006; Sato et al. 2005; Wang et al. 2007; Sato et al. 2007; Owen et al. 2008; Yagi et al. 2009; Harp et al. 2011; Martha et al. 2012; Gorum et al. 2013; Wartman et al. 2013; Chen et al. 2014; Xu et al. 2015).We have developed the coseismic landslide inventory map for the Gorkha earthquake based on the interpretation of the GF-1,GF-2, Landsat-8, Google earth satellite imageries and from field survey. We were able to map more than 4,000 landslides from the affected part.

A GIS-based landslide susceptibility map of the affected regions of Nepal was prepared using a statistical or probabilistic frequency ratio (FR) model and the coseismic landslide inventory map of the area. The model is easy to understand and it gives very good result. It has been applied widely for landslide susceptibility evaluation (Poudyal et al. 2010; Ozdemir and Altural 2013; Regmi et al. 2014; Shahabi et al. 2014; Wang et al. 2015; Anbalagan et al. 2015).

1 Study Area

Epicenter of the Gorkha earthquake was located at 28°15'07" N latitude and 84°07' 02" E longitude, while the landslides triggered off by the quake and its major aftershocks were scattered all around the mountainous regions of central Nepal. In this regard, we have selected a wide zone that has been affected by the seismically-induced mass movements. The study area covers about 15,456.49 km² (Figure 1a, b) and it ranges in altitude from 7,920 m to about 220 m with slope angle exceeding 85°. The main settlements are Gorkha, Barpak, Mugling, Manakamana, Naubise, Kakani, Nuwakot, Syaphrubese, Langtang, Rasuwagadi, Katunge, Nepalthok, Panchkhal, Chaku, Kodari, Larke, Langtang, Gaurishankar, and Giri Bazar (Figure 1b). The area is drained out by two major antecedent river systems, the Naryani to the west and the Sapta Koshi to the east. The main tributaries of the Narayani River in the study area are Trishuli, Budhi Gandaki, and Daraudi Khola, whereas those of the Sapta Koshi are the Sunkoshi, Balephi and Tamakoshi rivers (Figure 1b).

Geologically, Nepal lies at the central portion of the 2,400 km long Himalayan fold-and-thrust belt that resulted from the collision of the northward moving Indian Plate with the Eurasian Plate about 55 Ma (Dewey and Burke 1973). After the collision along the Indus–Tsangpo suture zone, the tectonic activity was partially transferred towards the south with the subsequent major events and the formation of many large faults, such as the MCT, Main Boundary Thrust (MBT), Himalayan Frontal Thrust (HFT) and the South Tibetan Detachment (STD). The Lesser Himalayan succession is bounded by the MCT in the north and the Neogene Siwaliks the south. It is composed essentially of Proterozoic low-grade metamorphic rocks and sedimentary sequences. The Higher Himalayan crystallines, consisting of medium- to high-grade rocks, are bounded by the STD in the north and the MCT in the south. The Tethyan Himalayan sequence, comprising the Proterozoic to Eocene sedimentary rocks, is bordered in the south by the STD.

The study area consists of rocks belonging to the Tethyan Himalaya sequence, Higher Himalaya crystallines, and the Lesser Himalayan succession (Dhital, 2015). The Tethyan Himalayan sequence of the Phulchoki Group (Stöcklin 1980) is represented by Tistung, Sopyang, Chitalng, and Godavari formations; while the Beimphedi Group is made up of the Marku Formation. On the other hand, rocks from the Higher Himalaya including Higher Himalayan Gneisses, Formation I, Formation II and Formation III are observed here. Besides, Annapurna Formation, Nilgiri Limestone, Pi Formation and some other Tethyan sedimentary rocks are observed in the study area. The Lesser Himalayan sequence of the region consists of Benighat Slates, some limestones, dolomites, Ulleri-type gneisses, and quartzites as well as phyllites and metasandstones of the Kuncha Formation and Birethanti Formation (Figure 2). The main rock types in the Tethyan Himalaya are limestone, dolomites, slates, and phyllite; while the Higher Himalaya is rich in schist, quartzite and
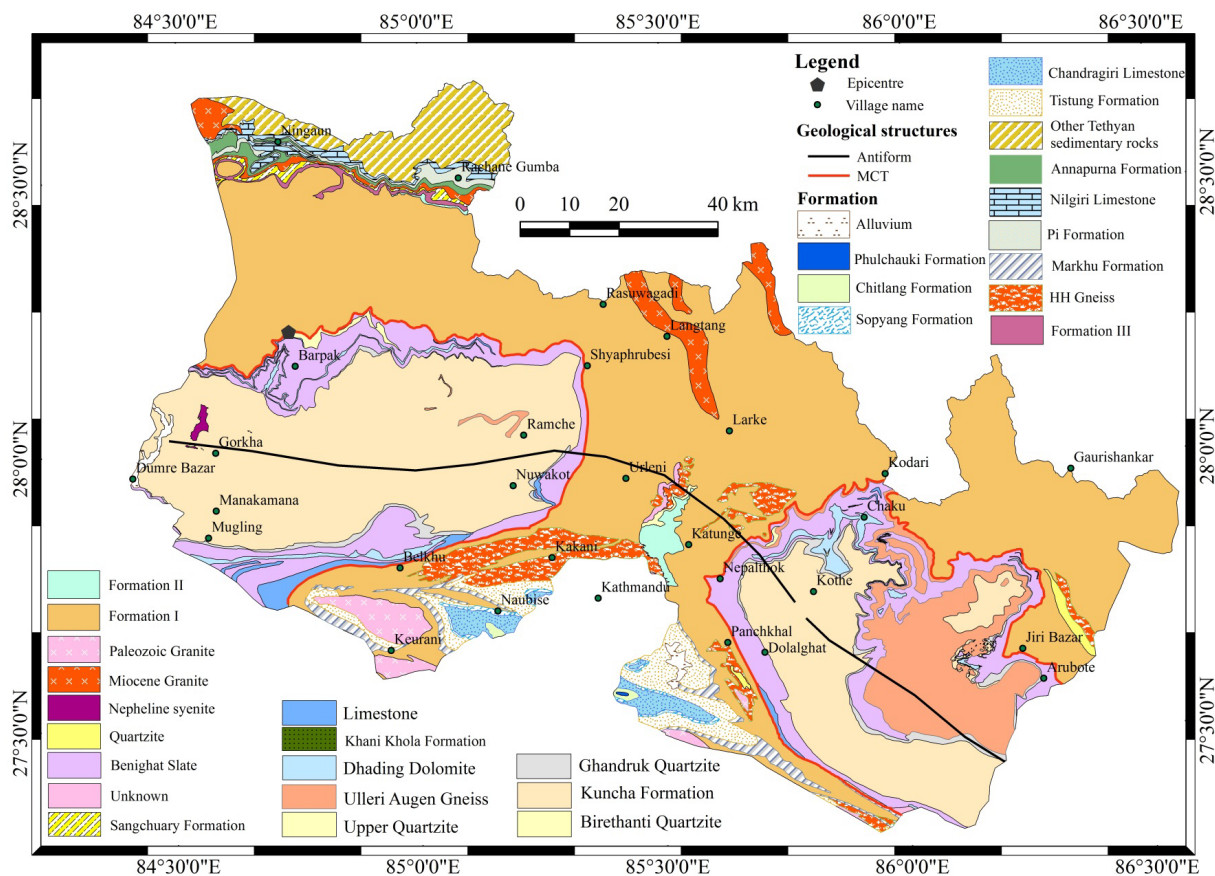

Figure 2 Geological map of the study area showing the distribution of various lithological units, Main Central Thrust and Great Midland Antiform (Modified from Dhital, 2015).

gneisses. Besides, several granite bodies are observed in both the Lesser Himalaya and Higher Himalaya. Also, a few nepheline syenite bodies crop up in the Lesser Himalaya, west of Gorkha.

The main geological structures in the study area are the MCT and the GMA. The MCT demarcates the study area into the eastern and western parts. The GMA extends east-west and passes through the central part of the area (Figure 2). Most of the epicenters of microseismic tremors in Nepal are clustered along the front of the Higher Himalayan Range (Avouac and Tapponnier 1993). The Gorkha earthquake also occurred along this front, i.e. at the footwall of the MCT. The earthquake created about 160 km long rupture that propagated towards the east, following the core of the GMA. The rupture extends through the Kuncha Formation of the Lesser Himalaya, consisting mainly phyllites and metasandstones with sporadic amphibolite bands. This formation is more than 4 km thick and comprises chlorite–sericite slates, phyllites, schists, quartzites, carbonates, and a few bands of augen or banded gneiss. The epicenter of main shock lies within the younger Benighat Slates (Dhital 2015). The hanging wall of the rupture zone is made up of the Higher Himalayan succession. A majority of aftershocks are located around the MCT and the GMA.

2 Data and Methodology

The methodology consists of data preparation for the susceptibility evaluation of the coseismic landslides and the techniques used for developing the susceptibility maps.

2.1 Data

To prepare a landslide susceptibility map of the earthquake-affected region, we have used satellite images as well as digital topographic model, land use data, and drainage and road maps provided by the Department of Survey, Government of Nepal (GoN). The geological data were collected from the published maps, whereas the seismic data were taken from the USGS website to construct spatial database from which the relevant factors were extracted. An earthquake-induced landslide inventory map of the region was developed from the field survey and the interpretation of remotely sensed data. Then various factor maps were compared with the landslide map for the susceptibility assessment of the region (Guzzetti et al. 1999; Ercanoglu and Gokceoglu 2004).

A digital elevation model (DEM) with a resolution of 20 m * 20 m is used for the present study. From the DEM, several thematic data layers, including the maps of slope angle, slope aspect, curvature, elevation and relative relief were derived using the Spatial Analyst tool in ArcGIS 10.2. On the other hand, lithology as well as the position of folds and faults was extracted from the geological map. Seismic data were used to extract the information on the PGA, distribution of the earthquake, and the distance to landslides from epicenters of the main shock and aftershocks exceeding a magnitude of 6.5. As the rupture surface is not exposed, it was not considered in the present analysis. We also used the distance from the MCT and GMA to the nearest mass movement, because the earthquake was indirectly related to the MCT and the rupture was supposed to follow the trend of GMA. In addition, the drainage map was used to obtain the distance to the nearest landslide from a river. All these factor maps were proposed to derive the spatial relationship between the given factor class and the seismically-induced landslides.

2.1.1 Landslide inventory

A landslide inventory is a map showing the distribution of landslide in an area. These maps are essential for the preparation of landslide susceptibility, hazard and risk maps of a region (Cardinali et al. 2006; Guzzetti et al. 2005; Guzzetti et al. 2012; van Westen et al. 2008). Different techniques can be used in developing landslide inventories depending on the purpose, area of the study, and the available resources to carry out the study (Guzzetti et al. 2012). For very large area, where the topography is very rough and is not easily assessable, it is not possible to carry out detailed fieldwork to develop the inventory map. Thus, remote sensing images are valuable tools in such areas. In this study, we have used different remote sensing images followed by a rapid field assessment to develop a coseismic landslide inventory map of the area affected by the

Gorkha earthquake. The earthquake triggered landslides were identified by manual image interpretation. Four kinds of remote sensing images were utilized in this research, landsat-8 ETM image with resolution of 15 m, GF-1 image with resolution of 2 m, GF-2 image with resolution of 0.8 m and Google Earth imageries. Landsat-8 ETM images before the earthquake cover the whole earthquake-effected area were taken as the base images (Figure 3a). Landslide-3 ETM images after the earthquake were used to identify the landslides by comparing with the base images (Figure 3b). GF-1 images and GF-2 images with higher resolution were utilized in the area where higher numbers of landslides have occurred (Figure 3c), and part of the landslides data were validated by the field work. Besides, Google Earth images were extensively used to develop the inventory map of the area. Walk over survey was conducted along Araniko Highway and the highway joining Rasuwagadi from Nuwakot. During this process, all the newly developed landslides were mapped. Besides, we conducted helicopter survey immediately after the Gorkha earthquake for initial survey of the mountain hazard, including landslides. Thus, from the satellite image analysis and fieldwork, more than 4,000 coseismic landslides were identified. However, only 3,716

landslides were included in the present study as the remaining landslides are located in China. Out of 3,716 landslides, 2,973 (about 80%) landslides were used for model training and the remaining 20% landslides were laid aside for validating purpose.

From the coseismic landslide inventory map of the area, it is seen that the size of the largest landslide is about 9,982 m^2 and the smallest one is less than 20 m^2. The coseismic landslides cover an area of about 15.93 km^2. From the analysis of the
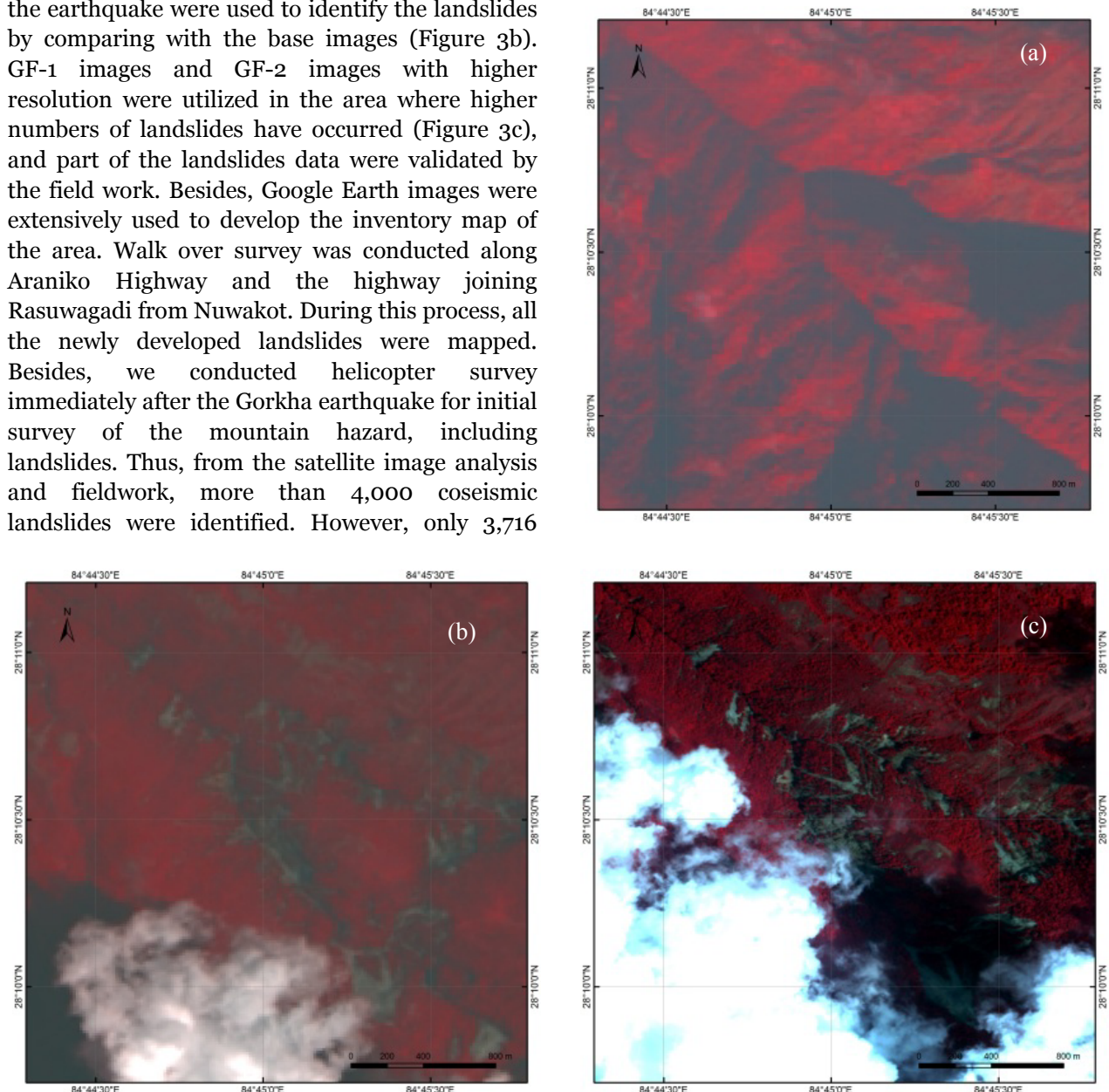

Figure 3 Remote sensing images before and after the earthquake were utilized to identify earthquake triggered landslides: (a) landsat-8 ETM image before the earthquake (Acquired Date: 2014-12-07, resolution: 15 m); (b) Landsat-3 ETM image after the earthquake (Acquired Date: 2015-05-23, resolution: 15 m) (c) GF-2 remote sensing image (Acquired Date: 2015-05-13, resolution: 0.8 m).

inventory map, it is seen that the highest densities of coseismic landslides occur mainly along river valleys of Bhote Koshi River, Balefi River, Trishuli River and Budhi Gandaki River where the main shock and two largest aftershocks followed by several aftershocks occurred (Kargel et al. 2016). The earthquake triggered landslides are mainly shallow slides and most of them are of rock slide and rock fall types.

Figure 4 shows some of the photographs of coseismic landslides taken during the fieldwork. A partial landslide dam is seen in the Bhote Koshi River due to a coseismic landslide (debris slide) that had occurred after the Gorkha earthquake (Figure 4a). Several slides were observed on slopes near Kodari. It is close to the MCT, where the 6.7 magnitude aftershock had occurred. Cloud of dust is seen here due to the sliding mass (Figure 4b). Most part of the road section was blocked here due to the falling rock mass from the slope. Several slides are observed along the Trishuli River, on the

way to Rasuwagadi from Nuwakot (Figure 4c). Here, mostly sallow slides are distributed all along the river valley. Figure 4c shows the road blockade along Pasang Lhamu Highway connecting Nepal and China (China–Nepal border). It is seen that a car had been hit by the falling rocks here (Figure 4d). These situations were observed all along the road sections connecting Nepal and China.

2.1.2 Topographical factors

In the study area, most of the landslides occurred on steep upper valley slopes of the hilly terrain, while the gentler lower slopes suffered from very less or no failures. The landslide occurrence in an area is strongly dependent of the slope, as an increase in gradient causes the increase in the level of gravity-induced shear stress in the hillslope materials, thus making them prone to failure (Oh and Lee 2011). The slope gradient in the study area ranges from 0°–85° and it is divided into eight classes.

Figure 4 Photographs of some landslides taken immediately after the Gorkha earthquake. (a) Partial damming of the Bhote Koshi River due to a coseismic landslide (debris slide); (b) Smoke of dust flowing into the air due to a sliding mass; (c) Several sallow landslides observed along Trishuli River on the way to Rasuwagadi from Nuwakot after the earthquake; (d) Rock fall along the Kathmandu-Rasuwagadi road section completely blocking the traffic.

Slope aspect, another important factor considered to be influential in the instability of a region, is defined as the compass direction of the slope and it controls the factors such as exposure to sunlight, land use, soil saturation, and discontinuities (Yalcin 2008). The aspect in this study is classified into nine classes.

The plan curvature is the rate of change of aspect and it is concave for a positive value, convex for a negative value, and is flat for zero value. It is important for the susceptibility evaluation, since it represents topographic convergence or divergence, controlling the flowing water through the slope.

The instability in a region is also controlled by its altitude. Usually, landslides are present at higher altitudes due to the influence of gravity. In the present study, the elevation is divided in to 8 classes.

We also analyzed the association between the relative relief of the area and the coseismic landslides. In the present study, relative relief varies between 0 to 661 m/km². Following five classes of relative relief (a) very low relief (<19), (b) low relief (19-34), (c) moderate relief (34-52), (d) high relief (53-80) and (e) very high relief (>80) were considered for this study. This classification was based on natural break.

2.1.3 Seismic factors

We have used the Peak Ground Acceleration (PGA) map of the 25 April Gorkha earthquake and the distance to epicenter of the mainshock and large (exceeding Mw 6.0) aftershocks. A string of aftershocks was immediately followed the main shock from its epicenter near Barpak to a region about 120 km east within 40 km wide area. It generated 553 aftershocks of local magnitude greater than 4.0 within the first 45 days (Adhikari et al. 2015). The two large aftershocks (>6.0 Mw) immediately followed the mainshock, while the largest (7.3 Mw) aftershock occurred after 17 days, i.e. on 12 May, 2015. PGA is a measure of earthquake acceleration of the ground recorded at a site on an accelerometer during a particular earthquake (Douglas 2003). During an earthquake, the short-lived strong ground motion produces imbalance within the hillslope materials, producing several slope failures. Thus, the occurrences of coseismic landslides is directly influenced by the ground motion (Keefer 1984). The PGA map

(USGS 2015) was divided into eight categories following the published literatures (Figure 5).

The intensity of the earthquake decreases as the distance from the epicenter increases. Hence, the intensity was also considered an important factor for the coseismic landslips. In this study, we have used the epicenter data of the Gorkha earthquake and its three aftershocks exceeding Mw 6.0. The epicenter distance is divided in to 8 classes with equal intervals.

2.1.4 Geological factors

Geology strongly affects the occurrence of instability in a region. Lithology controls the distribution of landslides, as different compositional units have varying physical and chemical properties, including weathering intensity as well as bedrock fracturing and jointing. Similarly, geological structures, such as faults and folds, develop weak zones where a landslide can initiate. In the present study, we have used lithology, the distance from the MCT and the distance from GMA as the main geological factors for the development of several coseismic landslips. We have used the MCT and GMA as the factor maps, since the rupture surface is not exposed and is believed to partially follow the course of these two geological structures.

A lithological layer was developed by the modification the geological maps of Nepal (Dhital 2015) and the Annapurna–Manaslu–Ganesh Himal region (Colchen et al. 1986). The rocks were divided into 24 differed lithologiclal units (Figure 2). They are mainly classified into alluvium, Tethyan Sedimentary sequence, Higher Himalayan crystallines, and Lesser Himalayan sequence. These units exhibit varying geological and geotechnical properties as well as susceptibility to failure.

The MCT separates the Lesser Himalayan rocks from the overlying Higher Himalayan rocks. The Gorkha Earthquake occurred very close to the MCT, and most of the aftershocks were also distributed in its vicinity. Thus, it is considered to be an important factor triggering coseismic landslips. Besides, many large landslides are observed in the region around the MCT throughout the Himalaya. The fault distance map was divided into 8 classes with 1 km interval.

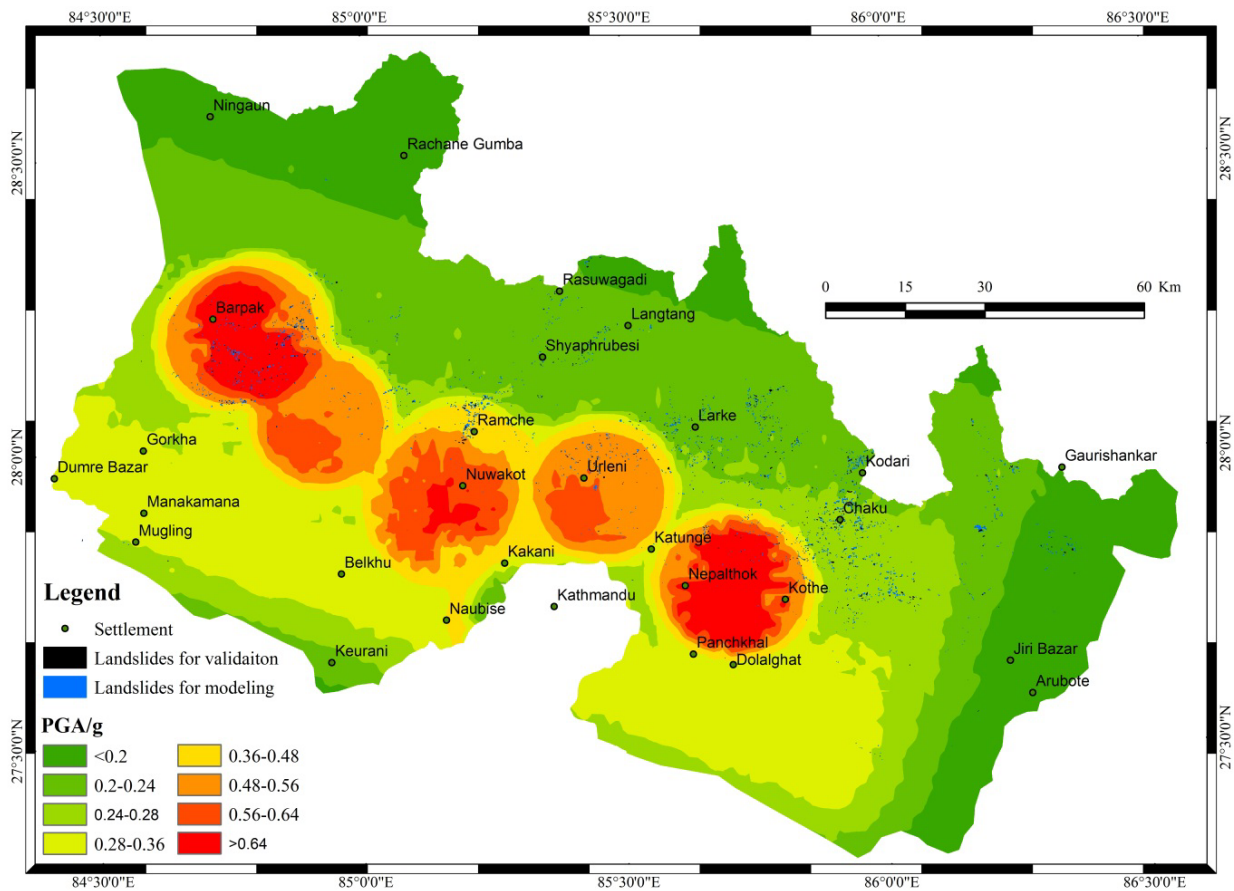The GMA is a regional-scale fold passing

Figure 5 Peak Ground Acceleration (PGA) map of the study area, along with the distribution of coseismic landslides.

through the Central part of the Himalaya. Since the Gorkha earthquake and the aftershocks were distributed close to this fold, it was considered being an important factor for the propagation of the rupture. Hence, a fold distance map was prepared and divided into 8 equal intervals.

2.1.5 Hydrological factors

Since most of the landslides are confined to river valleys, we applied the distance from a major drainage system as one of the influencing factors in the susceptibility evaluation. The river acts as an active erosional agent, making the slope steeper and saturating the materials lying with in the waterway (Gökceoglu and Aksoy 1996; Çevik and Topal 2003).

2.2 Susceptibility mapping

Among various statistical approach of landslide susceptibility mapping, we have adopted FR model for evaluating the susceptibility to

seismically-induced landslides in the region. It is a simple and easily understandable probabilistic model. The FR is defined as the ratio of the area where landslides occurred in the total study area to the ratio of the probabilities of a landslide occurrence to a non-occurrence for a given attribute (Bonham-Carter 1994; Pradhan and Lee 2010). This model is based on the observed relationships between each factor and the distribution of landslides. The FR can be expressed as,

$$FR = \frac{\frac{Npix(SX_i)}{\sum_{i=1}^{m} SX_i}}{\frac{Npix\,(X_j)}{\sum_{j=1}^{n} Npix(X_j)}} \qquad (1)$$

Where, $N_{pix}(SX_i)$ = number of pixels with landslide within class i of parameter variable X,

$N_{pix}(X_j)$ = number of pixels within parameter variable X_j,

m = number of classes in the parameter variable X_i,

n = number of parameters in the study area.

If this ratio is greater than 1, there is a greater correlation between a landslide and the specific factor's attribute; and vice versa. In order to calculate the FR of the factor map, the spatial analysis tool of ArcGIS 10.2 and a spreadsheet were used. These FR values were then used as weights for every factor map, which were then added together using the spatial analysis tool of ArcGIS software to get the LSI map as given below;

$$LSI = \sum FR \ldots \ldots \ldots \ldots \ldots (2)$$

Where, LSI is the landslide susceptibility index. The final landslide susceptibility map was developed by dividing the LSI map into 5 different classes.

3 Results

3.1 Correlation between coseismal landslide and each factor map

The distributions of landslides in each class of factor maps were analyzed using the spatial analysis tool of ArcGIS 10.2. The plot of FR in each class of each factor map is shown in Figure 6 (detailed data are listed in Appendix 1). This FR value can assess the effect of certain class on coseismic landslide occurrence.

If we considered the slope angle, then the correlation between the slope angle and FR value clearly indicates that the higher the slope angle, higher is the FR value (Figure 6a). This in turn indicates that steep slopes have the higher landslide susceptibility probability. As evident from fieldwork, most of the landslides were of rock-fall type occurring on steep slope. Thus, from this it is clear that the steep slopes are very prone to coseismic landslides in the study area. Similarly, in the case of slope aspect, it is seen that the FR value increases from the east-facing slope, becomes maximum for the south-facing one, and then gradually decreases towards the west-facing slope (Figure 6b). This explains that the south facing slopes have higher probability of landslide occurrence. This is mainly due to the exposure to sun rays, rainfall frequency (as the north facing slope is considered to be rain shadow zone) and human influence (is more in these slope due to the sunlight exposure). Mechanical, chemical and biological weathering is more intense on the southward facing slopes than the northward facing slopes. Thus, it becomes clear that the south facing slopes are more susceptible to coseismic landslide susceptibility than north facing slopes. In the case of curvature, concave and convex slopes higher FR value (Figure 6c), indicating greater correlation with the coseismic landslides. Hollows are characteristics of concave curvature, and surface water can converge as it moves downslope in such areas (Reneau and Dietrich 1987). These hollows concentrate groundwater, which then leads to increased landslide susceptibility. Sato et al. (2007) indicated that convex slopes are prone to large coseismic landslides. Thus, from Figure 6c, it is seen that both the concave and convex slope are more prone to coseismic landslide susceptibility. Similarly, in the case of altitude, it is seen that most of the landslides are confined to an altitude range of 2,500 to 3,500 m, with maximum at 3,000 m (Figure 6d). As the earthquake and most of its aftershocks were concentrated within this altitude, most of the coseismic landslides are observed here. Besides, it is seen that most of the landslides are concentrated along higher mountain slopes, rather than river valleys. This is mainly due to fact that the seismic body and the shear wave create inertial force within the mountain slope thus making the higher slope more prone to coseismic landslides. Relative relief greatly controls the occurrence of coseismic landslides within the study area. From Figure 6e, it is seen that the FR rapidly increases as the relative relief increases, indicating that higher relief areas are more prone to coseismic landslides. PGA, another important factor considered for the susceptibility evaluation, shows a very good correlation with landslides. From the analysis, it is seen that the FR increases with the increasing PGA values (Figure 6e). Comparison with the felt earthquake intensity, 0.6 and higher PGA indicate violent to extreme shacking. This can thus generate large number of coseismic landslides in steep mountain slopes. In the present study area, the FR is highest for PGA >0.64. In the case of distance from epicenter, the FR is highest within 10 km from the epicenter of the mainshock and its major aftershocks (Figure 5f), indicating that more earthquake induced landslides are closely related to the shacking of the ground during the earthquake. Beyond this distance, the FR ratio
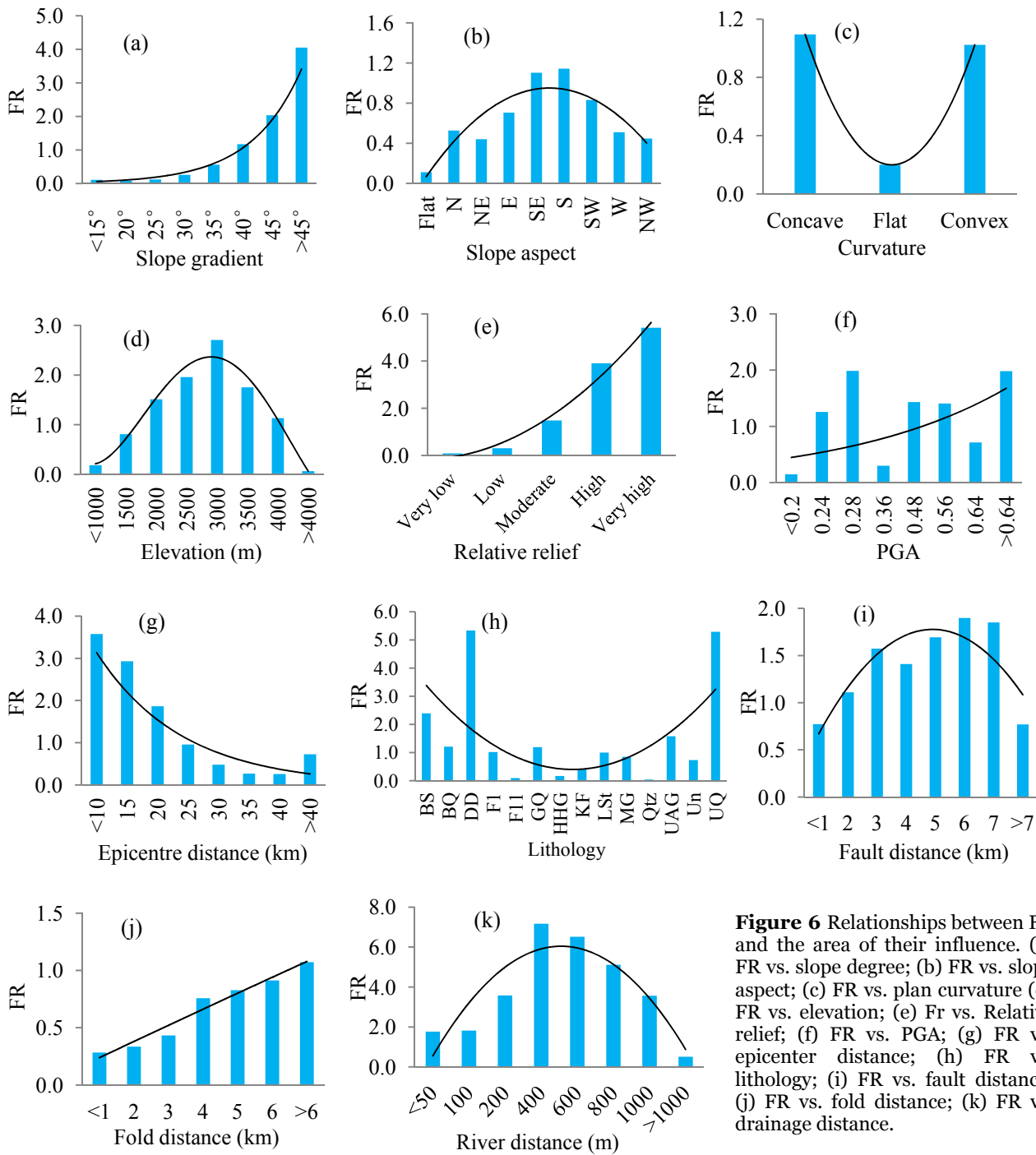
Figure 6 Relationships between FR and the area of their influence. (a) FR vs. slope degree; (b) FR vs. slope aspect; (c) FR vs. plan curvature (d) FR vs. elevation; (e) Fr vs. Relative relief; (f) FR vs. PGA; (g) FR vs. epicenter distance; (h) FR vs. lithology; (i) FR vs. fault distance; (j) FR vs. fold distance; (k) FR vs. drainage distance.

gradually decreases and becomes less than 1 beyond 20 km from the epicenters of the mainshock and aftershocks (Figure 6f).

From the analysis it is seen that the Upper Quartzite (UQ) and Dhading Dolomite (DD) have the highest landslide susceptibility probability as indicated by the FR value (>5). The UQ and DD mainly consist of quartzite and dolomite. They are highly fractured and jointed, and they have

developed steep slopes making them prone to rock fall. Similarly, the Benighat Slate (BS) has also higher potential for landslide susceptibility (FR>2) (Figure 6g). BSs are mostly consisting of soft rocks, as slates and phyllites and they are highly prone to landslides. Besides, Birethanti Quartzite (BQ), Ghandruk Quartzite (GQ), and Ulleri Augen Gneisses (UAG) have FR higher than 1, indicating good correlation with the coseismic landslides.

Most of these formations contain highly fractured and jointed quartzite and gneisses making them prone to rock slide and rock fall. On the other hand, there are many rock formations that are not affected by the quake. It is mainly due to their lithological characteristics and their geomorphological position. The distance from MCT was also used as one of the influential factors in triggering of coseismic landslides in the study area. The value FR is greater than 1 for up to 35 km, but it sharply decreases beyond 35 km and decreases to less than 1 at distance greater than 40 km (Figure 6h). This is presumably due to the fact that the rupture surface follows the MCT and most of the aftershocks are located close to this fault. Besides, we evaluated the role of fold (GMA) in the susceptibility evaluation of coseismic landslides. From the analysis, it is seen that the fold distance does not show a good correlation with the landslide susceptibility in the region (Figure 6i). This is mainly due to the fact that the GMA passes through low altitude area, with gentle topography as well as the rupture is not exposed on the surface.

FR values are greater than 1 up to a drainage distance of 1000 m, but beyond that they becomes less than 1 (Figure 6j). The river valleys have created very steep slopes, and these steep slopes are very prone to slope failure. Therefore, it is clear that the river network in the area had played positive role in the formation of the coseismic landslides.

3.2 Landslide susceptibility maps

The relationship between the landslides, landslide-conditioning factors, and their FR are shown in Figure 6. The statistically derived FR values of each class of the factor map were assigned to the respective classes of each factor maps to produce multiclass weighted maps. These multiclass weighted maps were overlaid in order to calculate a landslide susceptibility index map (Eq. 3). Kayastha (2015) have shown the effect of influencing factors in the susceptibility evaluation by excluding some of the factors during the final raster calculation process in Eq. 2. The susceptibility index map changes when the input factors are changed (Kayastha et al. 2015; Jadda et al. 2009). In the present study, we tried to see the effect of various factors in the susceptibility of

coseismic landslides. For this, we developed susceptibility map from topographic, geologic and seismic factors (Figure 7a), topographic and geologic factors (Figure 7b), all the factors (Figure 7c) and from topographic, geological and seismic factors (excluding relief and fold) (Figure 7d).

The performance of each susceptibility map was carried out using the success rate curve (Chung and Fabbri2003). For this purpose, the total landslide data was first divided into 80% and 20% for training the model and predicting the accuracy of the developed model. The success rate curves were developed from the training data. In order to calculate the area under the curve (AUC), the LSI index map was subdivided into 100 equal parts and it was crossed with both the training data. From this, the cumulative percentage of the training data was calculated for the LSI classes. The AUC was calculated for different susceptible maps (a) with all the conditioning factors, (b) from geological, topographic and seismic factors, (c) with only topographic and geological factors and (d) with topographic, geological and seismic factors (excluding relief and fold) (Figure 8). From figure, it is seen that there is only slight difference in the four curves, however the best result is shown by the LSI with topographic, geological and seismic factors (excluding relief and fold) having the area under curve 0.8766, equivalent to the success rate accuracy of 87.66%. Thus, from this we have used the most influencing factors for the susceptibility assessment of the region including topographic factors (excluding relief), geological factors (excluding fold distance) and seismic factors to derive the final landslide susceptibility zonation map using eq. (3).

$$LSM_{FR} = FR_{slope} + FR_{aspect} + FR_{curvature} + FR_{elevation} + FR_{PGA} + FR_{epicentre\ distance} + FR_{lithology} + FR_{fault\ distance} \qquad (3)$$

This map was than reclassified into five different susceptible classes (natural break) following published literatures (Figure 9). It is seen that the very low, low, moderate, high and very high susceptible zones occupy 23%, 32%, 26%, 14% and 5% respectively of the total study area and they contain 0.76%, 7.31%, 21.35%, 32.81% and 37.78% of the total landslide area. In addition, it is seen that very high and high susceptible zones contain 11.25 km² of the landslide area, which is 70% of the
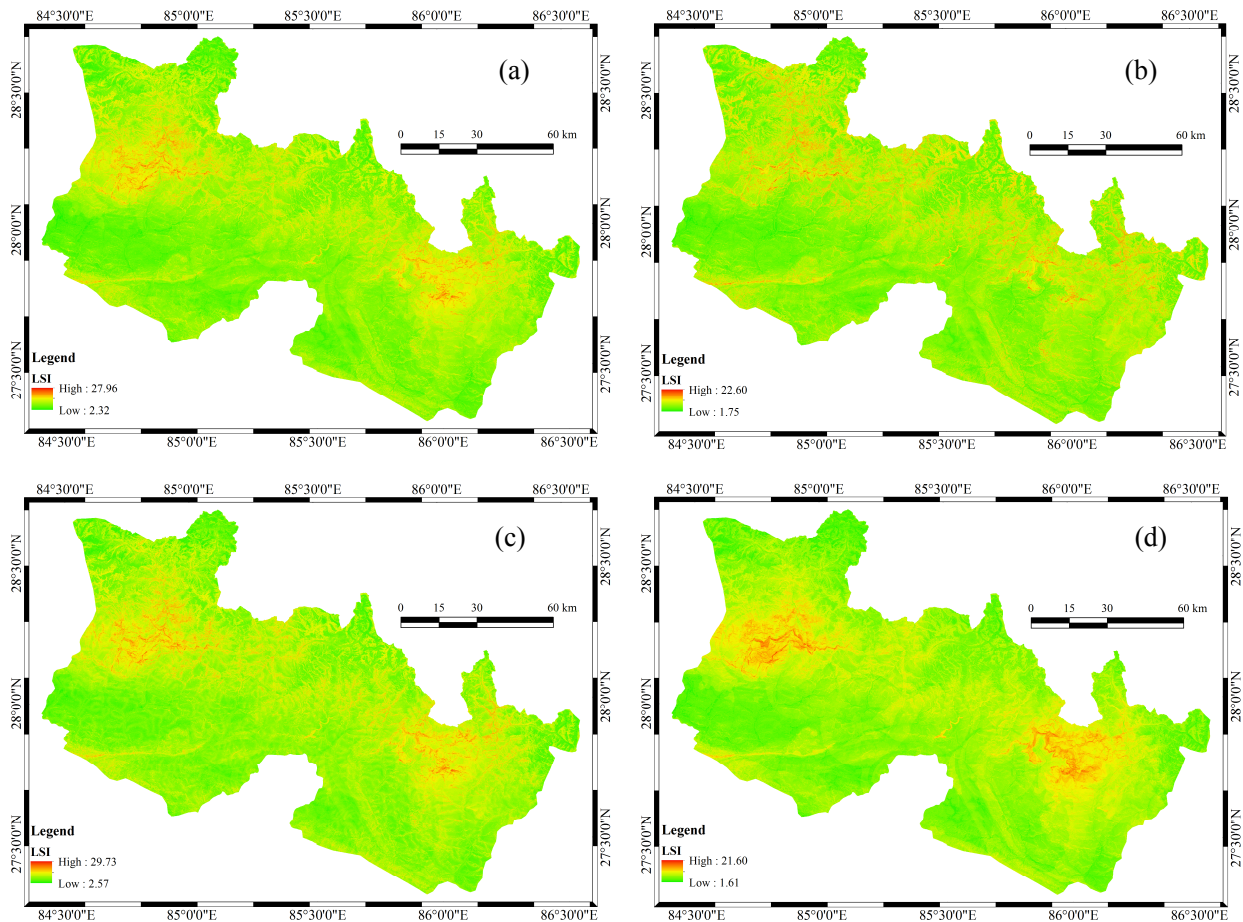
Figure 7 Landslide susceptibility index (LSI) maps of the study area derived from (a) Geological, seismological and topographical factors; (b) Topographical and geological factors; (c) With all the factors including drainage; and (d) With geological, seismological and topographical factors (excluding fold and relief).

total landslide area (Table 1). The area around Barpak where the epicenter of the Gorkha earthquake lies is in very high susceptible zone.
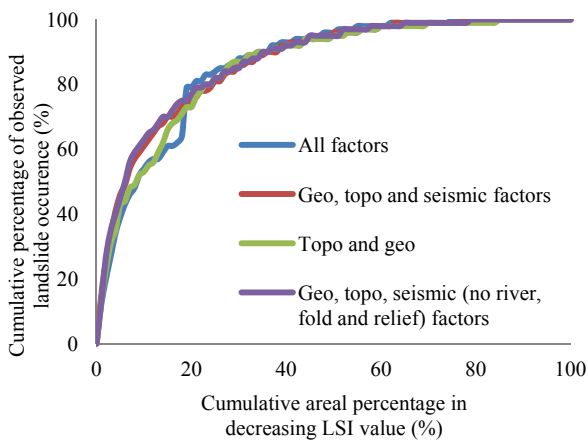

Figure 8 Success rate curves of four landslide susceptibility index maps showing that the map with geologic, topographic and seismic factors (without fold, relative relief and river distance) have better performance.

Similarly, the area around Kodari, Barabise, and Kothe are under high to very high susceptibility class. From Figure 9, it is seen that the central part of the study area is under moderate to low susceptible zone. Thus, it seen that most of the eastern and western part of the study area fall in high susceptible zone. Because the epicenter of the Gorkha earthquake was at Barpak and large aftershocks were scattered in the eastern part of the study area, landslide susceptibility is quite high in this portion. In addition, most part of Highway joining Nepal and China through Kodari belongs to very high to high susceptible class, the highway through Rasuwa Gadhi falls under moderate to high susceptible zone, and the highway connecting southern part of Nepal with Kathmandu lies in low susceptible zone (Figure 9). Since most of the very high to high susceptible zones lie in areas with very steep slopes, within the PGA values of >0.64, and in the Upper Quartzite, Dhading Dolomite and
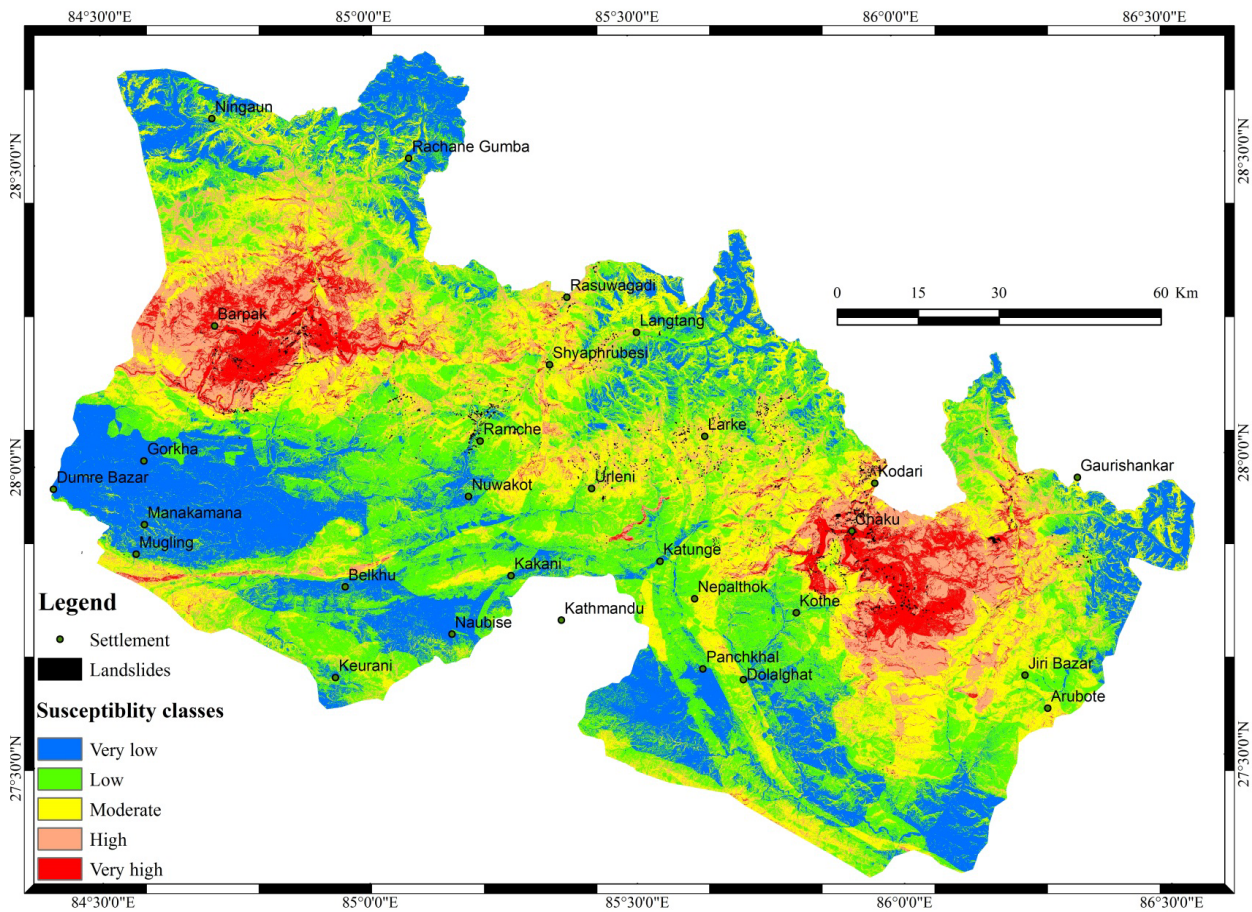
Figure 9 Landslide susceptibility map of the earthquake affected area showing the distribution of coseismic landslides.

Table 1 Area, % area of landslide susceptibility zone and landslide within each susceptibility zone; and density of landslide within each susceptibility zone

Susceptibility class			Landslide		
Classes	Area (km²)	%	Area (km²)	% in area	Density
Very low	3742.85	24.22	0.12	0.76	0.000
Low	4895.10	31.67	1.16	7.31	0.000
Moderate	3882.03	25.12	3.40	21.35	0.001
High	2099.58	13.58	5.23	32.81	0.002
Very high	836.93	5.41	6.02	37.78	0.007

Benighat Slates; it is clear that the slope, lithology and PGA significantly control landslide susceptibility in the region. As the footwall of the MCT rests on the Benighat Slates, the fault also becomes influential in the susceptibility zonation (Figure 9).

The prediction capability of the susceptibility model was done using the 20% landslide data that was not used for training the model and which was kept for predicting the accuracy of the developed model (Chung and Fabbri 2003). The prediction rate curve shows the AUC of 0.8687 (Figure 10).

This means that the prediction rate is 86.87%, which is considered to be quite promising.

4 Conclusions and Discussions

We used the landslide data collected from the remote sensing images and fieldwork to develop a coseismic landslide susceptibility map of the area affected by the Gorkha earthquake. The inventory of landslide was randomly divided into training and testing data sets. Coseismic landslide
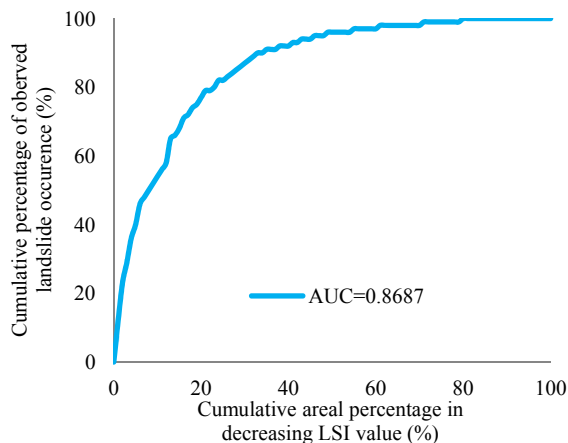
Figure 10 Prediction rate curve shows that landslide susceptibility map with geology, topography and seismic factor (excluding fold and relief) have very good performance with prediction rate of 86.87%.

susceptibility map was developed from the training datasets, using eight differing landslide condition factors, and the model was successfully validated using the validation dataset. Also, from the analysis, it is seen that topography, geology and seismic factors have played more prominent role in the formation of coseismic landslides in the Gorkha earthquake affected regions. The susceptibility map thus produced can be useful for the planners and engineers for relocating the people from hazardous zone to safer places. Besides, the map can also be helpful in implementing development works in this earthquake prone region.

There have been serious concerns over coseismic landslides due to their potential for heavy destruction. In this regard, several researchers have done extensive studies in the field of earthquake-induced landslides (Harp and Jibson 1996; Keefer, 2002; Yen et al. 2009; Ren and Lin 2010; Dai et al. 2011; Alfaro et al. 2012; Xu et. al. 2015).

The Gorkha earthquake and its subsequent aftershocks triggered thousands of landslides. The impact of such coseismic landslides could be observed as far as the Everest region. A similar earthquake of magnitude 7.6 occurred on 8 October 2008 in Kashmir, Pakistan. It generated about 2,500 coseismic landslides (Shafique et al. 2016), a number similar to that of the Gorkha earthquake. On the other hand, the Weinchuan earthquake in China, with a magnitude akin to the Gorkha earthquake had generated more than 60,000 coseismic landslides (Ren and Lin 2010; Qi et al. 2010; Dai et al. 2011; Xu et al. 2013). The lesser number of landslide occurrence in Nepal is mainly due to the following factors.

The Weinchuan earthquake developed a thrust fault, whose rupture surface was exposed, while the Gorkha earthquake had a concealed rupture surface. Owing to this, the surface materials were less disturbed by the Gorkha earthquake and hence fewer landslides occurred. The rupture surface of the Gorkha earthquake is about 160 km long, while that of the Weinchuan earthquake is more than 300 km. The propagation of rupture surface generates secondary geohazards (such as landslides and surface deformations), which are clustered along the exposed rupture line. Thus, a smaller number of coseismic landslips in Nepal can be attributed to the shorter rupture length. The investigation of earthquake-induced landslides has shown the hanging wall – foot wall effect (Hung and Li 2013). Generally, the number of coseismic landslides is higher in the hanging wall than in the footwall of the rupture surface. In the Gorkha earthquake, the hanging wall of the rupture surface consists of massive and resistant Higher Himalayan rocks. The area around the rupture surface and its footwall exhibits relatively gentle topography. In contrast, the area surrounding the rupture surface of the Weinchuan earthquake is very rugged with steep slopes. The constituent soft sedimentary rocks of that region are also intensely deformed and contain many thrusts and folds. Thus, earthquakes with a similar magnitude can generate a varying number of landslides, depending upon the depth of rupture surface and its propagation direction as well as the governing geological, geomorphic, hydrological, and anthropogenic factors.

Acknowledgement

Electronic Supplementary Materials: Supplementary materials (Appendix 1) are available in the online version of this article at http://dx.doi.org/10.1007/s11629-015-3688-2.

References

Adhikari LB, Gautam UP, Koirala BP, et. al. (2015) The aftershock sequence of the 2015 April 25 Gorkha–Nepal earthquake. Geophysical Journal International 203: 2119-2124. DOI: 10.1093/gji/ggv412

Alfaro P, Delgado J, García-Tortosa FJ, et. al. (2012) Widespread landslides induced by the Mw 5.1 earthquake of 11 May 2011 in Lorca, SE Spain. Engineering Geology 137-138: 40-52. DOI:10.1016/j.enggeo.2012.04. 002

Anbalagan R, Kumar R, Lakshmanan K, et. al. (2015) Landslide hazard zonation mapping using frequency ratio and fuzzy logic approach, a case study of Lachung Valley, Sikkim. Geoenvironmental Disasters 2(1): 1-17. DOI: 10.1186/s40677-014-0009-y

Avouac JP, Tapponnier P (1993) Kinematic model of active deformation in central Asia. Geophysical Research Letters 20(10): 895-898. DOI:10.1029/93GL00128

Bonham-Carter G (1994) Preface. In: Graeme FB-C (ed) Computer Methods in the Geosciences, vol Volume 13. Pergamon, pp xiii-xvii. DOI: 10.1016/B978-0-08-042420-0.50005-5

Cardinali M, Galli M, Guzzetti F, et. al. (2006) Rainfall induced landslides in December 2004 in south-western Umbria, central Italy: types, extent, damage and risk assessment. Natural Hazards and Earth System Sciences 6(2): 237-260. DOI: 10.5194/nhess-6-237-2006

Çevik E, Topal T (2003) GIS-based landslide susceptibility mapping for a problematic segment of the natural gas pipeline, Hendek (Turkey). Environmental Geology 44(8): 949-962. DOI: 10.1007/s00254-003-0838-6

Chen XL, Yu L, Wang MM, et. al. (2014) Brief Communication: Landslides triggered by the Ms = 7.0 Lushan earthquake, China. Natural Hazards and Earth System Sciences 14(5): 1257-1267. DOI: 10.5194/nhess-14-1257-2014

Chigira M, Wu X, Inokuchi T, Wang G (2010) Landslides induced by the 2008 Wenchuan earthquake, Sichuan, China. Geomorphology 118(3-4): 225-238. DOI: 10.1016/j.geomorph.2010.01.003

Chigira M, Yagi H (2006) Geological and geomorphological characteristics of landslides triggered by the 2004 Mid Niigta prefecture earthquake in Japan. Engineering Geology 82(4): 202-221. DOI: 10.1016/j.enggeo.2005.10. 006

Chung CJ, Fabbri A (2003) Validation of Spatial Prediction Models for Landslide Hazard Mapping. Natural Hazards 30(3): 451-472. DOI: 10.1023/B:NHAZ.0000007172.62651.2b

Colchen M, Le Fort P, Pêcher A (1986) Annapurna–Manaslu–Ganesh Himal. Centre National de la Recherches Scientifique, Special Publication, Paris

Collins BD, and Jibson RW (2015) Assessment of existing and potentiallandslide hazards resulting from the April 25, 2015 Gorkha, Nepal earthquakesequence (ver. 1.1, August 2015): U.S. Geological Survey Open-File Report 2015-1142, p. 50. DOI: 10.3133/ofr20151142

Dai FC, Xu C, Yao X, et. al. (2011) Spatial distribution of landslides triggered by the 2008 Ms 8.0 Wenchuan earthquake, China. Journal of Asian Earth Sciences 40: 883-895. DOI: 10.1016/j.jseaes.2010.04.010

Dewey JF, Burke ACA (1973) Tibetan, Variscan, and Precambrian basement reactivation: products of continental collision. The Journal of Geology 81(6): 683-692.

Dhital MR (2015) Geology of the Nepal Himalaya: Regional Perspective of the Classic Collided Orogen (Regional Geology Reviews). Springer; 2015 edition (February 12, 2015).

Douglas J (2003) Earthquake ground motion estimation using strong-motion records: a review of equations for the estimation of peak ground acceleration and response spectral ordinates. Earth-Science Reviews 61(1-2): 43-104. DOI: 10.1016/S0012-8252(02)00112-5

Ercanoglu M, Gokceoglu C (2004) Use of fuzzy relations to produce landslide susceptibility map of a landslide prone area (West Black Sea Region, Turkey). Engineering Geology 75(3-4): 229-250. DOI: 10.1016/j.enggeo.2004. 06. 001

Gökceoglu C, Aksoy H (1996) Landslide susceptibility mapping of the slopes in the residual soils of the Mengen region (Turkey) by deterministic stability analyses and image processing techniques. Engineering Geology 44(1-4): 147-161. DOI: 10.1016/S0013-7952(97)81260-4

Gorum T, van Westen CJ, Korup O, et. al. (2013) Complex rupture mechanism and topography control symmetry of mass-wasting pattern, 2010 Haiti earthquake. Geomorphology 184: 127-138. DOI: 10.1016/j.geomorph. 2012. 11.027

Guzzetti F, Carrara A, Cardinali M, Reichenbach P (1999) Landslide hazard evaluation: a review of current techniques and their application in a multi-scale study, Central Italy. Geomorphology 31(1-4): 181-216. DOI: 10.1016/S0169-555X (99)00078-1

Guzzetti F, Mondini AC, Cardinali M, et. al. (2012) Landslide inventory maps: New tools for an old problem. Earth-Science Reviews 112(1-2): 42-66. DOI: 10.1016/ j.earscirev. 2012.02. 001

Guzzetti F, Reichenbach P, Cardinali M, et. al. (2005) Probabilistic landslide hazard assessment at the basin scale. Geomorphology 72(1-4): 272-299. DOI: 10.1016/j.geomorph. 2005.06.002

Hagen T (1969) Report on the geological survey of Nepal. Volume 1: Preliminary Reconnaissance. Denkschiiften der Schweizerischen Naturforschenden Gesellschaft, Band LXXXVI/1, p. 185. (with ageological map)

Harp EL, Jibson RW (1996) Landslides triggered by the 1994 Northridge, California, earthquake. Bulletin of the Seismological Society of America 86(1 Suppl. B).

Harp EL, Keefer DK, Sato HP, et al. (2011) Landslide inventories: The essential part of seismic landslide hazard analyses. Engineering Geology 122(1-2): 9-21. DOI: 10.1016/j. enggeo.2010.06.013

Huang RQ, Li WL (2013) Co-Seismic Fault Effects of Landslides Triggered by Wenchuan Ms 8.0 Earthquake, China. In: Huang Y, Wu F, Shi Z, et al. (eds.), New Frontiers in Engineering Geology and the Environment. Springer Berlin Heidelberg. pp 1-11

Jadda M, Shafri HZM, Mansor SB, et. al. (2009) Landslide susceptibility evaluation and factor effect analysis usingprobabilistic-frequency ratio model. European Journal of Scientific Research 33(4): 654-668.

Kargel JS, Leonard GJ, Shugar DH, et. al. (2016) Geomorphic and geologic controls of geohazards induced by Nepal's 2015 Gorkha earthquake. Science 351(6269): aac8353. DOI: 10.1126/science.aac8353

Kayastha P (2015) Landslide susceptibility mapping and factor effect analysis using frequency ratio in a catchment scale: a case study from Garuwa sub-basin, East Nepal. Arabian Journal of Geosciences 8: 8601-8613. DOI: 10.1007/s12517-015-1831-6

Keefer DK (1984) Landslides caused by earthquakes. Geological Society of America Bulletin 95(4): 406-421.

Keefer DK (2002) Investigating landslides caused by earthquakes—a historical review. Surveys in Geophysics 23(6): 473-510. DOI: 10.1023/A:1021274710840

Khazai B, Sitar N (2004) Evaluation of factors controlling earthquake-induced landslides caused by Chi-Chi earthquake and comparison with the Northridge and Loma Prieta events. Engineering Geology 71(1-2): 79-95. DOI: 10.1016/S0013-7952(03)00127-3

Lee CT, Huang CC, Lee JF, et. al. (2008) Statistical approach to earthquake-induced landslide susceptibility. Engineering Geology 100(1-2): 43-58. DOI: 10.1016/j. enggeo.2008.03. 004

Martha TR, Kerle N, van Westen CJ, et. al. (2012) Object-oriented analysis of multi-temporal panchromatic images for creation of historical landslide inventories. ISPRS Journal of Photogrammetry and Remote Sensing 67: 105-119. DOI: 10.1016/j.isprsjprs.2011.11.004

Ministry of Home Affairs (MoHA), Government of Nepal (2015) Available online at: http://www.moha.gov.np/

Oh HJ, Lee S (2011) Landslide susceptibility mapping on Panaon Island, Philippines using a geographic information system. Environmental Earth Sciences 62(5): 935-951. DOI: 10.1007/s12665-010-0579-2

Owen LA, Kamp U, Khattak GA, et. al. (2008) Landslides triggered by the 8 October 2005 Kashmir earthquake. Geomorphology 94(1-2): 1-9. DOI: 10.1016/j.geomorph. 2007.04.007

Ozdemir A, Altural T (2013) A comparative study of frequency ratio, weights of evidence and logistic regression methods for landslide susceptibility mapping: Sultan Mountains, SW Turkey. Journal of Asian Earth Sciences 64: 180-197. DOI: 10.1016/j.jseaes.2012.12.014

Poudyal C, Chang C, Oh H-J, et al. (2010) Landslide susceptibility maps comparing frequency ratio and artificial neural networks: a case study from the Nepal Himalaya. Environmental Earth Sciences 61(5): 1049-1064. DOI: 10.1007/ s12665-009-0426-5

Pradhan B, Lee S (2010) Delineation of landslide hazard areas on Penang Island, Malaysia, by using frequency ratio, logistic regression, and artificial neural network models. Environmental Earth Sciences 60(5): 1037-1054. DOI: 10.1007/ s12665-009-0245-8

Qi S, Xu Q, Lan H, et. al. (2010) Spatial distribution analysis of landslides triggered by 2008.5.12 Wenchuan Earthquake, China. Engineering Geology 116(1-2): 95-108. DOI: 10.1016/j. enggeo.2010.07.011

Regmi A, Yoshida K, Pourghasemi H, et. al. (2014) Landslide susceptibility mapping along Bhalubang — Shiwapur area of mid-Western Nepal using frequency ratio and conditional probability models. Journal of Mountain Science 11(5): 1266-1285. DOI: 10.1007/s11629-013-2847-6

Regmi AD, Cui P, Dhital MR, Zou Q (2016) Rock fall hazard and risk assessment along Araniko Highway, Central Nepal Himalaya. Environmental Earth Sciences 75: 1-20. DOI: 10.1007/s12665-016-5905-x

Ren Z, Lin A (2010) Co-seismic landslides induced by the 2008 Wenchuan magnitude 8.0 Earthquake, as revealed by ALOS PRISM and AVNIR2 imagery data. International Journal of Remote Sensing 31: 3479-3493. DOI: 10.1080/01431161003727770

Reneau SL, Dietrich WE (1987) The importance of hollows in debris flow studies; Examples from Marin County, California. In: Costa JE, Wieczorek GF (eds.), Debris Flows/Avalanches: Process, Recognition, and Mitigation. Geological Society of America, Boulder, Colorado. Reviews in Engineering Geology VII: 165-180. DOI: 10.1130/REG7-p165

Sato H, Hasegawa H, Fujiwara S, et. al. (2007) Interpretation of landslide distribution triggered by the 2005 Northern Pakistan earthquake using SPOT 5 imagery. Landslides 4(2): 113-122. DOI: 10.1007/s10346-006-0069-5

Sato H, Sekiguchi T, Kojiroi R, et. al. (2005) Overlaying landslides distribution on the earthquake source, geological and topographical data: the Mid Niigata prefecture earthquake in 2004, Japan. Landslides 2(2): 143-152. DOI: 10.1007/s10346-005-0053-5

Shahabi H, Khezri S, Ahmad BB, Hashim M (2014) Landslide susceptibility mapping at central Zab basin, Iran: A comparison between analytical hierarchy process, frequency ratio and logistic regression models. CATENA 115: 55-70. DOI: 10.1016/j.catena.2013.11.014

Shafique M, van der Meijde M, Khan MA (2016) A review of the 2005 Kashmir earthquake-induced landslides; from a remote sensing prospective. Journal of Asian Earth Sciences 118: 68-80. DOI: 10.1016/j.jseaes.2016.01.002

Stocklin J (1980) Geology of Nepal and its regional frame: Thirty-third William Smith Lecture. Journal of the Geological Society 137(1): 1-34. DOI:10.1144/gsjgs.137.1.0001

U.S. Geological Survey, Earthquake Hazards Program (2015) Available online at: http://earthquake.usgs.gov (Accessed on 20 May 2015)

van Westen CJ, Castellanos E, Kuriakose SL (2008) Spatial data for landslide susceptibility, hazard, and vulnerability assessment: An overview. Engineering Geology 102(3-4): 112-131. DOI: 10.1016/j.enggeo.2008.03.010

Wang HB, Sassa K, Xu WY (2007) Analysis of a spatial distribution of landslides triggered by the 2004 Chuetsu earthquakes of Niigata Prefecture, Japan. Natural Hazards 41(1): 43-60. DOI: 10.1007/s11069-006-9009-x

Wang LJ, Guo M, Sawada K, et. al. (2015) A comparative study of landslide susceptibility maps using logistic regression, frequency ratio, decision tree, weights of evidence and artificial neural network. Geosciences Journal 20(1): 117-136. DOI: 10.1007/s12303-015-0026-1

Wartman J, Dunham L, Tiwari B, et al. (2013) Landslides in eastern Honshu induced by the 2011 off the Pacific coast of Tohoku Earthquake. Bulletin of the Seismological Society of America 103(2B): 1503-1521.

Xu C, Xu X, Yao X, Dai F (2013) Three (nearly) complete inventories of landslides triggered by the May 12, 2008 Wenchuan Mw 7.9 earthquake of China and their spatial distribution statistical analysis. Landslides 11: 441-461. DOI: 10.1007/s10346-013-0404-6

Xu C, Xu X, Shyu JBH (2015) Database and spatial distribution of landslides triggered by the Lushan, China Mw 6.6 earthquake of 20 April 2013. Geomorphology 248: 77-92. DOI: 10.1016/j.geomorph.2015.07.002

Yagi H, Sato G, Higaki D, et. al. (2009) Distribution and characteristics of landslides induced by the Iwate–Miyagi Nairiku Earthquake in 2008 in Tohoku District, Northeast Japan. Landslides 6(4): 335-344. DOI:10.1007/s10346-009-0182-3

Yalcin A (2008) GIS-based landslide susceptibility mapping using analytical hierarchy process and bivariate statistics in Ardesen (Turkey): Comparisons of results and confirmations. CATENA 72(1): 1-12. DOI: 10.1016/j.catena. 2007.01.003

Yamagishi H, Iwahashi J (2007) Comparison between the two triggered landslides in Mid-Niigata, Japan by July 13 heavy rainfall and October 23 intensive earthquakes in 2004. Landslides 4(4): 389-397. DOI:10.1007/s10346-007-0093-0

Yin Y, Wang F, Sun P (2009) Landslide hazards triggered by the 2008 Wenchuan earthquake, Sichuan, China. Landslides 6(2): 139-152. DOI:10.1007/s10346-009-0148-5